Phase Stability of the Earth-Abundant Tin Sulfides SnS, SnS_2 and Sn_2S_3

Lee A. Burton and Aron Walsh*

Centre for Sustainable Chemical Technologies, Department of Chemistry, University of Bath, Bath, UK

E-mail: a.walsh@bath.ac.uk

Abstract

The various phases of tin sulfide have been studied as semiconductors since the 1960s and are now being investigated as potential earth-abundant photovoltaic and photocatalytic materials. Of particular note is the recent isolation of zincblende SnS in particles and thin-films. Herein, first-principles calculations are employed to better understand this novel geometry and its place within the tin sulfide multiphasic system. We report the enthalpies of formation for the known phases of SnS, SnS_2 and Sn_2S_3 with good agreement between theory and experiment for the ground-state structures of each. Whilst theoretical x-ray diffraction patterns do agree with the assignment of the zincblende phase demonstrated in the literature, the structure is not stable close to the lattice parameters observed experimentally, exhibiting an unfeasibly large pressure and a formation enthalpy much higher than any other phase. *Ab initio* molecular dynamics simulations reveal spontaneous degradation to an amorphous phase much lower in energy, as Sn(II) is inherently unstable in a regular tetrahedral environment. We conclude that the known rocksalt phase of SnS has been mis-assigned as zincblende in the recent literature.

*To whom correspondence should be addressed

Introduction

Photovoltaic (PV) devices are of growing importance due to increasing population and diminishing reserves. Today, PV technology predominantly uses silicon as an absorber material, but due to the low optical absorption coefficient, up to 500 μm thick films are needed to absorb significant fractions of visible light. More optimal absorber materials need less than 5μm thickness,[1] giving rise to so called thin-film technologies that require less material and much cheaper processing conditions than silicon, indeed the lowest among commercial PV technologies.[2] Successful examples include the commercially available cadmium telluride (CdTe) and copper-indium-gallium-selenide (CIGS) cells that have achieved record efficiencies close to 20%.[3] Unfortunately tellurium, indium and gallium are rare and expensive, alternatives must be sought if PV is ever to scale up to the level of energy generation provided by non-renewable methods: tera-watt production.

Quaternary blends of more common elements can circumvent the issue of precursor availability and cost; where properties are tailored to PV applications by varying the stoichiometry of individual components.[4] Most notable among these is Cu_2ZnSnS_4 (CZTS) which has achieved efficiencies of greater than 10%.[5] As an alloy of Cu_2S, ZnS and SnS_2, element availability is not a concern, but controlling the component ratios can be difficult. It has been shown that the desirable phase of CZTS occupies just a small fraction of the overall phase space for the system,[6,7] and has little or no thermodynamic barrier to phase separation.[8]

Herein, we consider tin sulfide, which is one of the components of CZTS and is itself attractive for PV applications because it is abundant, environmentally benign, and inexpensive.[9] For example, tin extraction and importation to the European Union has an associated carbon footprint of less than one tenth of that of gallium[3] and has an occurrence of 2 ppm on the the earth's crust.[10]

Tin sulfide single crystals have been grown by the Bridgman method and chemical vapour transport;[11,12] and thin-films can be formed by chemical vapour deposition,[13] chemical bath deposition,[14] atomic layer deposition,[15] electrodeposition,[16] sulfurisation of tin films,[17] solid-state

[3]Data obtained from 'tin at regional storage' system process and 'gallium, semiconductor grade, at regional storage' system process of the ecoinvent database using an endpoint recipe within SimaPro7 software. May 2012.

multilayer synthesis,[18] and successive ionic layer adsorption and reaction.[19] Nano-structures reported to date include, but are not limited to, nanoporous SnS frameworks by templated synthesis,[20] nanodisks by electrodeposition,[21] nanosheets by pyrolysis of single source precursor,[22] nanoflowers by hydrothermal synthesis,[23] nanobelts by a molten salt solvent method,[24] and fullerene-like nanoparticles by laser ablation.[25]

Significantly, it has been claimed that zincblende (ZB) tin monosulfide micro-particles have been synthesised,[26] and deposited as thin-films.[10] This would allow for increased compatibility with existing technologies based on II-VI and III-V tetrahedral semiconductors. For example, the current generation of thin-film solar cells relies on a clean interface between the absorber material and the zincblende structured cadmium sulfide window layer. ZB structures also tend to exhibit a direct fundamental bandgap and large optical absorption coefficients, which could serve to increase tin sulfide's performance as a PV material.

Most work agrees that orthorhombic SnS has a direct optical bandgap of $1.30-1.43$ eV,[27,28,29] while older work[30] and a recent theoretical study advocate an indirect bandgap at 1.07 eV.[31] Regardless, all investigations agree on an effective optical absorption onset around 1.4 eV, which coincides with the optimum band gap for maximum efficiency according to the Shockley-Queisser limit within the AM 1.5 solar spectrum.[32] SnS also has a higher optical absorption coefficient than CdTe and other existing PV materials,[27,33] with intrinsic *p*-type conductivity considered to be brought about by the formation of tin vacancies according to the defect reaction:[34]

$$\mathrm{Sn_{Sn}} \longrightarrow \mathrm{V''_{Sn}} + 2\,\mathrm{h^{\bullet}} + \mathrm{Sn(s)}$$

The ease of forming these vacancies is a potential source of discrepancy between reported properties and why, despite being an ideal candidate for PV applications, SnS devices have not yet surpassed 1.3% efficiency.[27]

In this paper, we report the enthalpies of formation of the known phases of the tin sulfides and compare the relative stability of each. The values are calculated using a first-principles electronic structure method based on density functional theory. While good agreement is found between theory and the known ground-state phases, there are deviations between the expected properties of

zincblende SnS and those obtained using the level of theory employed in this work, calling into question the validity of recent experimental assignments. Indeed, the known rocksalt (RS) phase of SnS gives rise to the same powder diffraction pattern, with a cubic lattice constant similar to that identified for the ZB phase, which leads us to conclude that the latter structures have been incorrectly assigned in recent experiments.

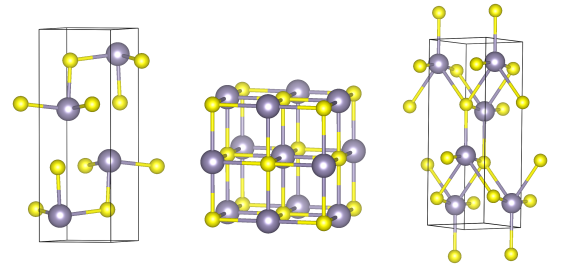

(a) SnS *Pnma* (b) SnS *Fm-3m* (c) SnS *Cmcm*

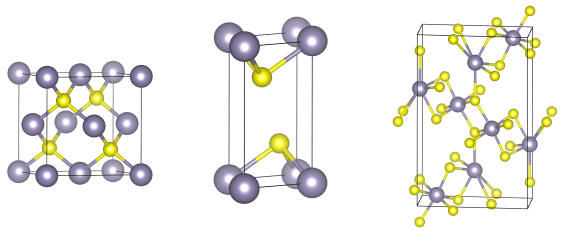

(d) SnS *F-43m* (e) SnS_2 *P-3m1* (f) Sn_2S_3 *Pnma*

Figure 1: the crystal structures of tin (grey) mono-sulfide (yellow) and the ground-state structures of SnS_2 and Sn_2S_3.

Computational Methods

The unique crystal structures of all tin sulfide phases were identified from the inorganic crystal structure database (ICSD). Density functional theory (DFT) as implemented in the Fritz Haber Institut *ab initio* molecular simulations (FHI-AIMS) package was used to calculate the equilibrium geometry and total energy for each structure.[35–37] To describe the effect of electron exchange and correlation, the semi-local generalized gradient approximation (GGA) was applied within the density functional of Perdew, Burke and Ernzerhof optimised for solids (PBEsol).[38] Local numerical orbital basis sets were used along with periodic boundary conditions applied in 3 dimensions to

approximate bulk solids. A well-converged Tier-2 basis set was employed for each species, with scalar-relativistic effects treated at the scaled ZORA level of theory.[39] Finally the *k*-point density was checked for convergence to within 0.01 eV per formula unit.

All calculations were performed in closed shell configuration (restricted spin), with geometry relaxations undertaken using the Broyden-Fletcher-Goldfarb-Shanno (BFGS) algorithm and a force convergence criterion tolerance in all cases of 0.01 eV/Å.[40]

In order to assess dynamic phase stability, *ab initio* molecular dynamics (MD) simulations were carried out within the Nosé-Hoover thermostat of the NVT canonical ensemble. This approach combines DFT forces with classical Newtonian mechanics, and a time-step of 1 fs. The temperature ranges modelled were 300, 500, 700 and 1000 K. The systems were brought to equilibrium over 5 ps and quenched directly to 0 K, followed by the standard local optimization procedure.

Results

Crystal Structures

SnS preferentially crystallises in the orthorhombic herzenbergite structure, with the space group *Pnma*. In this structure, the Sn^{2+} ion coordinates to three S^{2-} ions, with the Sn $5s^2$ lone pair occupying the last position of a tetrahedral geometry, following the revised lone pair model.[41] Other phases of SnS that are of interest are the rocksalt structure grown under epitaxial strain,[42] the high temperature orthorhombic structure,[43] and the ZB structure first reported in 1962 from SnS evaporation onto rocksalt,[44] with further reports occurring only very recently.[10,26]

The different SnS geometries are shown in Figure 1 along with the ground-state structures of SnS_2 and Sn_2S_3. The low energy phase of SnS_2 is a hexagonal structure composed of SnS_2 trilayers, where the Sn(IV) ion is coordinated to six S ions in an octahedral environment, which is similar, for example, to that found in rutile-structured SnO_2. Alternate stacking of the trilayers results in a series of structural polytypes, as typified by the isostructural CdI_2 system.

The crystal structure of tin sesquisulfide is tetragonal and shares the same space group as the

ground-state phase of SnS. The structure is composed of Sn_2S_3 chains, with the Sn(IV) ions adopting chain-centre positions with octahedral coordination to S, and the Sn(II) ions adopting chain-end positions in the favoured trigonal-pyramidal arrangement. Hence, the coordination preferences of both Sn oxidation states can be simultaneously satisfied. The spacegroup labels for SnS correspond to the following structures: *Pnma*; the orthorhombic ground-state phase, *Fm-3m*; the rocksalt phase, *Cmcm*; the orthorhombic, high temperature phase and the *F-43m* zincblende phase.

Table 1: Reported structural parameters from X-Ray diffraction measurements and resultant geometries relaxed within DFT

Phase	Spacegroup	Experimental parameters			Ref.	Relaxed parameters (% error)		
		a	*b*	*c*		*a*	*b*	*c*
SnS	*Pnma*	11.32	4.05	4.24	[43]	11.11 (1.89)	3.99 (1.52)	4.24 (0.10)
SnS	*Fm-3m*	5.8	5.8	5.8	[45]	5.75 (0.87)	5.75 (0.87)	5.75 (0.87)
SnS	*F-43m*	5.845	5.845	5.845	[26]	6.43 (10.0)	6.43 (10.0)	6.43 (10.0)
SnS_2	*P-3m1*	3.64	3.64	5.89	[46]	3.66 (0.44)	3.67 (0.80)	6.06 (2.75)
Sn_2S_3	*Pnma*	8.87	3.75	14.02	[12]	8.80 (0.83)	3.77 (0.66)	13.83 (1.36)
SnO	*P4/n m m*	3.80	3.80	4.82	[47]	3.81 (0.26)	3.81 (0.26)	4.76 (1.09)
SnO_2	*P42/m n m*	4.74	4.74	3.19	[48]	4.77 (0.72)	4.77 (0.72)	3.22 (0.97)

Table 1 contains the lattice parameters for the different SnS phases. For the ground-state structures, the calculated lattice parameters are in excellent agreement with experiment, where the error is typically less than 2%. One exception is the *c* axis of SnS_2, which is overestimated to 2.75 % due to the non-bonding nature of the inter-layer interactions (van der Waals interactions are not well described at this level of theory). The *Cmcm* phase could not be stabilised as it undergoes a second-order phase transition to the ground-state *Pnma* structure, which is observed experimentally at 878 K.[49] A significant discrepancy is only observed between the calculated and measured lattice parameters for the ZB *F-43m* structure.

The equilibrium lattice parameter of the ZB phase is 10% larger than the reported value. This has been checked with other DFT functionals (local, semi-local and non-local variants) and implementations (*i.e.* the VASP code).[50] The calculated energy-volume curve is shown in Figure 2 alongside that of the rocksalt (*Fm-3m*) phase. The slope of the curves represents the effective pressure of the system, *i.e.* $P=-(\partial U/\partial V)_T$, which for the observed ZB lattice parameter corresponds

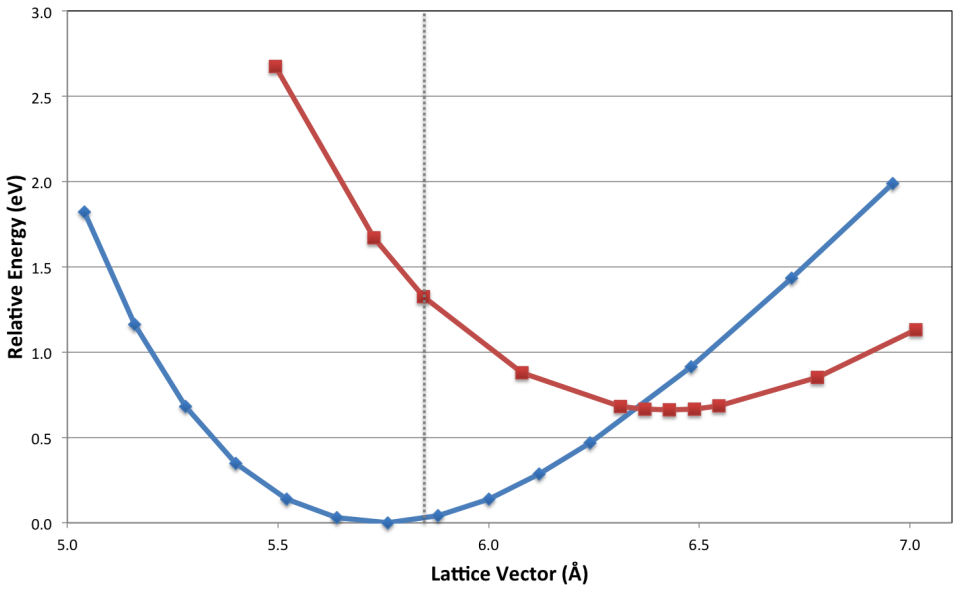

Figure 2: Energy-volume curve for zincblende (red) and rocksalt (blue) SnS. The reported lattice parameter of 5.845 Å is indicated with a vertical line.[26]

to an extremely large pressure of around 930 GPa , and can clearly not be representative of an equilibrium state. On the other hand, we direct the readers attention to the similarity between the experimental ZB lattice parameter and the equilibrium rocksalt lattice parameter.

The dynamic instability of the ZB phase was confirmed by a spontaneous distortion in MD simulations at room temperature (300 K), as well as the presence of large imaginary frequencies in phonon calculations. Three plausible explanations exist for this behaviour: (i) the actual phase found in experiment is not ZB; (ii) the phase is formed in a highly strained environment; (iii) the phase is stabilised by a high concentration of lattice defects. However, the large size of the particles reported by Greyson *et al.*,[26] lead us to conclude that explanation (i) is most likely.

Enthalpies of Formation

Enthalpies of formation are key to understanding the relative stabilities of a multi-phase system as they indicate which conformation the system would preferentially adopt. Indeed, simple thermodynamic arguments have been shown to play a fundamental role in the design, optimisation and performance of solar cell devices due to issues associated with phase mixing and separation across

interfaces.[51] The following results, obtained from DFT calculations, formally represent values at 0 K and do not account for any prohibitive kinetic barriers involved in structural change. We define the enthalpies according to the reaction $xSn(s) + yS(s) \longrightarrow Sn_xS_y$.

Table 2: Enthalpies of formation calculated in this work, and compared to experimental data where available

Phase	Spacegroup	ΔH_f^{DFT} (eV)	(kJ mol^{-1})	ΔH_f^{exp} (kJ mol^{-1})
SnS	*Pnma*	-1.03	-99.35	-100 to -108,[52,53]
SnS	*Fm-3m*	-0.95	-91.66	
SnS	*F-43m*	-0.29	-27.80	
SnS_2	*P-3m1*	-1.36	-130.99	-148 to -182[53,54,55]
Sn_2S_3	*Pnma*	-2.39	-230.35	-249 to -297[53,54,55]

The enthalpies of formation for tin mono-sulfide shown in Table 2 agree very well with experiment, whereas the formation enthalpies for SnS_2 and Sn_2S_3 deviate significantly. In the opinion of the authors, this result reflects more on the difficulty of obtaining phase pure materials experimentally than on the accuracy of the level of theory employed in this work, which is supported by the large variation in the measured enthalpies of formation.

The calculated enthalpy of formation for individual phases plotted against elemental composition affords a convenient method of comparing phase stabilities for any binary state. A convex hull is a plot of this kind, with the lowest energy states connected to form the base of a 'hull' and any higher energy states appearing above this line, is shown in Figure 3. The convex hull also indicates the energies of alternate composition ratios for that system.

Together with the results described in Table 2, the convex hull for the tin sulfides shows that ZB *(F-43m)* tin mono-sulfide should not be thermodynamically accessible under normal synthesis conditions; it lies 0.74 eV above the ground state *Pnma* phase. Considering that *Cmcm* SnS does not form below 878$\pm$5 K,[49] it is possible to see the relative magnitude of internal energy inherent to ZB SnS. The energy of the ZB phase is associated with the optimised lattice parameters reported in Table 1. Even higher energies are obtained for the ZB structure using experimental lattice constants, with the difference between them shown in Figure 2. In contrast, rocksalt SnS, while not the ground-state, should still be thermodynamically accessible.

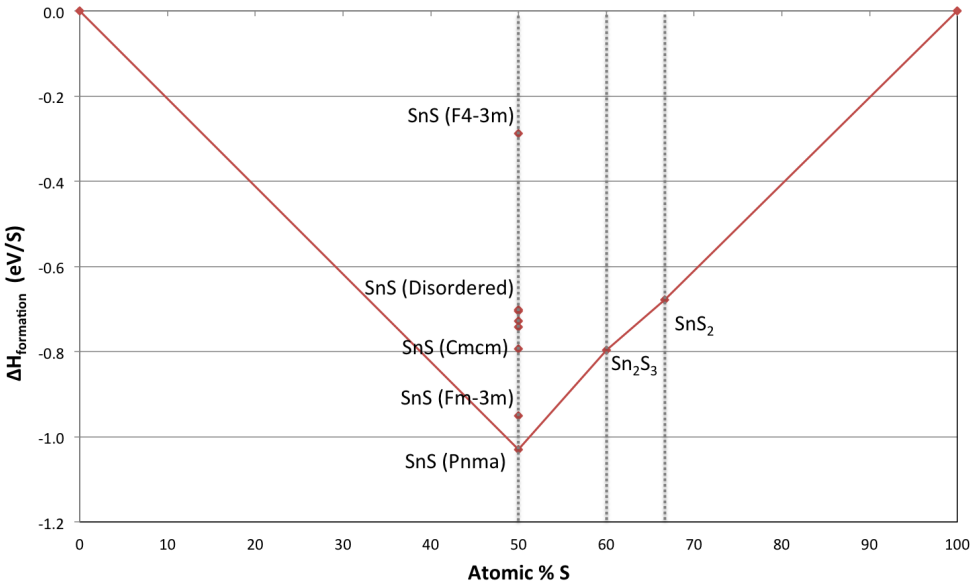

Figure 3: Convex hull showing enthalpy of formation against atomic percent of sulfur present in each phase.

Predicted X-Ray Diffraction Patterns

The predicted x-ray diffraction patterns for rocksalt and zincblende SnS, at the same lattice spacing, are shown in Figure 4. One can see that the peak positions and the reflections associated with each are equivalent, due to the common fcc crystal structure, and it would be possible to confuse the two. We cannot account for the preferential orientation of crystals due to the dependence of the growth process on nucleation,[56] but a powder diffraction of each would show that ZB SnS exhibits a stronger (111) reflection at 2θ =26.8 °, whereas rocksalt SnS would have a stronger (002) reflection at 2θ =31.0. In previous work the intensity ratios predicted for ZB SnS were not adhered to in ascribing the ZB structure from the diffraction pattern and this could be important in distinguishing between the two phases.[10] Both of these patterns correspond exactly with the peak positions of the XRD of ZB SnS reported by both Greyson *et al.* and Avellaneda *et al.* for nano-particulate and thin-film tin sulfides, respectively.[10,26]

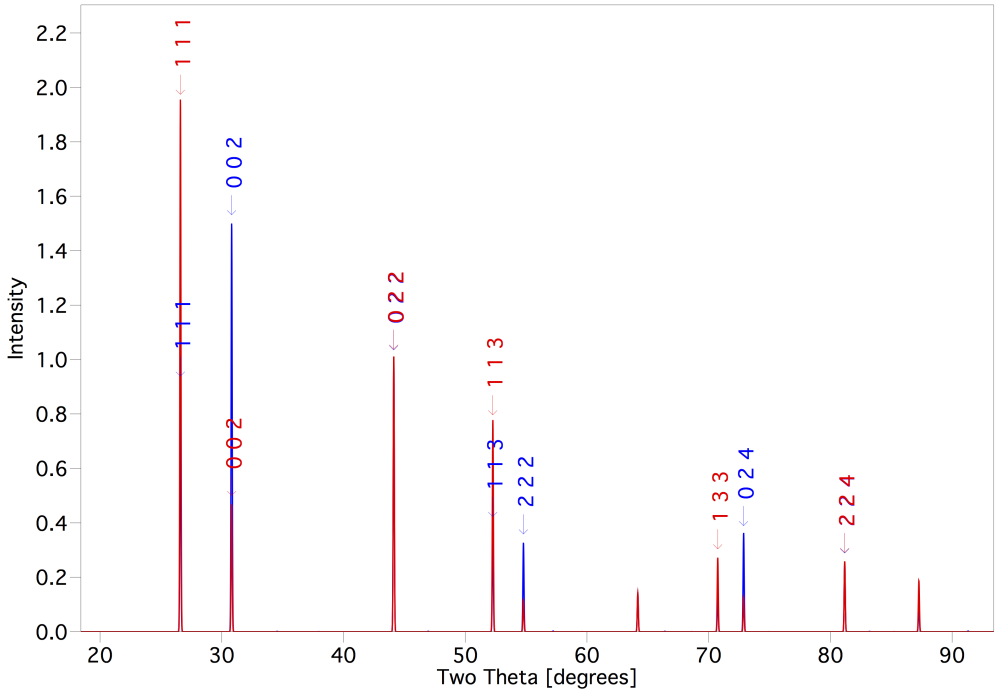

Figure 4: Predicted x-ray diffraction spectra for rocksalt (blue) and zincblende (red) SnS.

Discussion

Our calculations show very good agreement with observed crystal parameter values for the majority of the tin sulfide family of compounds, with the main outstanding issue being relating to the cubic zincblende phase of SnS.

The ZB mono-sulfide appears unusually high in energy and spontaneously distorts when allowed to relax even at room temperature. Quenching of the ZB (a $2 \times 2 \times 2$ 64-atom supercell) structure from temperatures of 300-1000 K resulted in a series of disordered phases, one of which is shown in Figure 5. The distribution in energy of these amorphous structures is shown in Figure 3. The amorphous structures all have energies more than 0.4 eV lower than ZB itself and contain predominantly three-fold coordinate tin in a trigonal pyramidal geometry. This is the typically adopted conformation of the ground-state tin sulfide structures, and one can see the orientation of the stereochemically active lone pairs on tin towards cavities in the lattice, as found for other tin compounds.[57,58]

It has been shown that the formation of an asymmetric electron density on Sn(II) is induced by

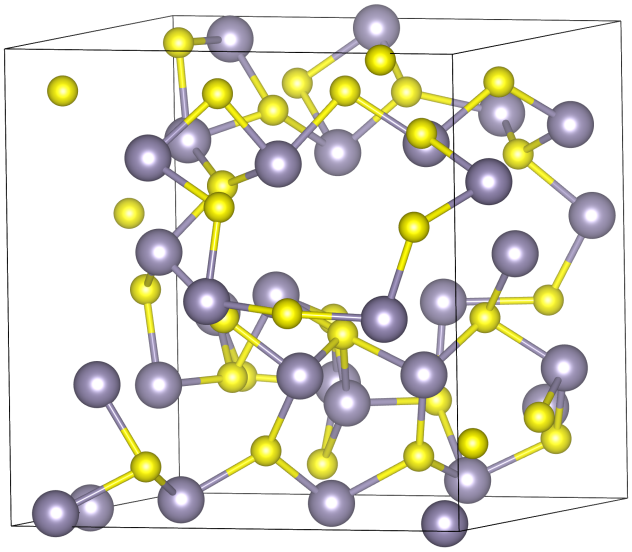

Figure 5: Structure of a typical amorphous SnS obtained upon quenching a MD simulation of the ZB phase.

a tetrahedral environment with sulfur, due to orbital interactions (Sn5s−5p hybridisation).[59] The same interaction is prohibited by the inversion symmetry of rocksalt,[60] lending further credence to the phase instabilities reported in this work. It should be noted that the tetrahedral geometry is known, and stable, for the Sn(IV) oxidation state, where the valence electronic configuration is $5s^0 5p^0$, i.e. the s orbitals are formally empty. Examples range from molecular $SnCl_4$ to metal sulfides such as CZTS and metal phosphides such as $ZnSnP_2$.[61]

Finally, the predicted diffraction patterns shown in this work highlight a possible source of confusion in the recent studies of tin sulfide. We propose that the known rocksalt phase has been mis-assigned as zincblende.

Conclusions

In conclusion, we have assessed the structural and thermodynamic properties of SnS, SnS_2 and Sn_2S_3 from first-principles calculations. Good agreement with experiment is obtained, with the exception of zincblende SnS, which is predicted to be thermodynamically and dynamically unstable. The predictions match the expectation from textbook inorganic chemistry that high-symmetry

coordination environments are adopted by the Sn(IV) ion, but the Sn(II) ion favours asymmetric environments of low coordination. A spontaneous distortion from tetrahedral to trigonal-pyramidal arrangement is observed to occur. Recent experimental reports could be explained by: (i) a structural misassignment; (ii) highly-strained crystallites; (iii) high concentrations of lattice defects forming a superlattice structure. However, based on the equivalent nature of reflections in the RS and ZB diffraction patterns, we propose that the known rocksalt phase of SnS has been misassigned as zincblende in recent reports.

Acknowledgement

The authors thank Kieran Molloy, Chris Bowen and Laurie Peter (Bath) for useful discussions and Gilles Dennler (IMRA-Europe) for suggesting the topic. AW acknowledges support from the Royal Society University Research Fellowship scheme and LB is funded by EPSRC (Grant No. EP/G03768X/1). Access to the HECToR supercomputer was facilitated through membership of the HPC Materials Chemistry Consortium, which is funded by EPSRC (Grant No. EP/F067496) Images of chemical structure were made using VESTA software.[62]

References

(1) Nelson, J. *The Physics of Solar Cells*; Imperial College Press, 2003.

(2) Fthenakis, V. *Renew. Sust. Energ. Rev.* **2009**, *13*, 2746 – 2750.

(3) Green, M. A.; Emery, K.; Hishikawa, Y.; Warta, W. *Prog. Photovoltaics Res. Appl.* **2011**, *19*, 84–92.

(4) Chen, S.; Gong, X. G.; Walsh, A.; Wei, S. H. *Phys. Rev. B* **2009**, *79*, 165211.

(5) Bag, S.; Gunawan, O.; Gokmen, T.; Zhu, Y.; Todorov, T. K.; Mitzi, D. B. *Energy Environ. Sci.* **2012**, *5*, 7060–7065.

(6) Chen, S.; Gong, X. G.; Walsh, A.; Wei, S. H. *Appl. Phys. Lett.* **2010**, *96*, 021902–3.

(7) Chen, S.; Yang, J. H.; Gong, X. G.; Walsh, A.; Wei, S. H. *Phys. Rev. B* **2010**, *81*, 245204.

(8) Zhai, Y. T.; Chen, S.; Yang, J. H.; Xiang, H. J.; Gong, X. G.; Walsh, A.; Kang, J.; Wei, S. H. *Phys. Rev. B* **2011**, *84*, 075213.

(9) Peter, L. M. *Philos. Trans. R. Soc. London, Ser. A* **2011**, *369*, 1840–1856.

(10) Avellaneda, D.; Nair, M. T. S.; Nair, P. K. *J. Electrochem. Soc* **2008**, *155*, D517–D525.

(11) Vyas, S. M.; Pandya, G. R.; Desai, C. F. *Indian J. Pure. Ap. Phy.* **1995**, *33*, 191–194.

(12) Cruz, M.; Morales, J.; Espinos, J. P.; Sanz, J. *J. Solid State Chem.* **2003**, *175*, 359–365.

(13) Kana, A. T.; Hibbert, T. G.; Mahon, M. F.; Molloy, K. C.; Parkin, I. P.; Price, L. S. *Polyhedron* **2001**, *20*, 2989 – 2995.

(14) Nair, P. K.; Nair, M. T. S.; Garcia, V. M.; Arenas, O. L.; Pena, Y.; Castillo, A.; Ayala, I. T.; Gomezdaza, O.; Sanchez, A.; Campos, J.; Hu, H.; Suarez, R.; Rincon, M. E. *Sol. Energ. Mat. Sol. C.* **1998**, *52*, 313–344.

(15) Kim, J. Y.; George, S. M. *J. Phys. Chem. C* **2010**, *114*, 17597–17603.

(16) Ghazali, A.; Zainal, Z.; Hussein, M. Z.; Kassim, A. *Sol. Energ. Mat. Sol. C.* **1998**, *55*, 237–249.

(17) Sugiyama, M.; Miyauchi, K.; Minemura, T.; Ohtsuka, K.; Noguchi, K.; Nakanishi, H. *Jpn. J. Appl. Phys.* **2008**, *47*, 4494–4495.

(18) Xu, Z.; Chen, Y. *Semicond. Sci. Tech.* **2012**, *27*, 035007.

(19) Ghosh, B.; Das, M.; Banerjee, P.; Das, S. *Appl. Surf. Sci.* **2008**, *254*, 6436–6440.

(20) Jiang, T.; Lough, A. J.; Ozin, G. A.; Young, D.; Bedard, R. L. *Chem. Mater.* **1995**, *7*, 245–248.

(21) Boonsalee, S.; Gudavarthy, R. V.; Bohannan, E. W.; Switzer, J. A. *Chem. Mater.* **2008**, *20*, 5737–5742.

(22) Zhang, Y.; Lu, J.; Shen, S.; Xu, H.; Wang, Q. *Chem. Commun.* **2011**, *47*, 5226–5228.

(23) Zhu, H.; Yang, D.; Zhang, H. *Mater. Lett.* **2006**, *60*, 2686 – 2689.

(24) Zhang, H.; Hu, C.; Wang, X.; Xi, Y.; Li, X. *J. Alloy. Compd.* **2012**, *513*, 1 – 5.

(25) Hong, S. Y.; Popovitz-Biro, R.; Prior, Y.; Tenne, R. *J. Am. Chem. Soc.* **2003**, *125*, 10470–10474.

(26) Greyson, E. C.; Barton, J. E.; Odom, T. W. *small* **2006**, *2*, 368 – 371.

(27) Reddy, K. R.; Reddy, N. K.; Miles, R. *Sol. Energ. Mat. Sol. C.* **2006**, *90*, 3041 – 3046.

(28) Noguchi, H.; Setiyadi, A.; Tanamura, H.; Nagatomo, T.; Omoto, O. *Sol. Energ. Mater. Sol. Cells* **1994**, *35*, 325 – 331.

(29) Sugiyama, M.; Murata, Y.; Shimizu, T.; Ramya, K.; Venkataiah, C.; Sato, T.; Reddy, K. T. R. *Jpn. J. Appl. Phys.* **2011**, *50*, 05FH03.

(30) Parenteau, M.; Carlone, C. *Phys. Rev. B* **1990**, *41*, 5227–5234.

(31) Vidal, J.; Lany, S.; d'Avezac, M.; Zunger, A.; Zakutayev, A.; Francis, J.; Tate, J. *Appl. Phys. Lett.* **2012**, *100*, 032104.

(32) Shockley, W.; Queisser, H. J. *J. Appl. Phys.* **1961**, *32*, 510–&.

(33) Ferekides, C. S.; Balasubramanian, U.; Mamazza, R.; Viswanathan, V.; Zhao, H.; Morel, D. L. *Sol. Energy* **2004**, *77*, 823 – 830.

(34) Albers, W.; Haas, C.; J. Vink, H.; Wasscher, J. D. *J. Appl. Phys.* **1961**, *32*, 2220.

(35) Hohenberg, P.; Kohn, W. *Phys. Rev.* **1964**, *136*, B864–B871.

(36) Kohn, W.; Sham, L. J. *Phys. Rev.* **1965**, *140*, A1133–A1138.

(37) Havu, V.; Blum, V.; Havu, P.; Scheffler, M. *J. Comput. Phys.* **2009**, *228*, 8367–8379.

(38) Perdew, J. P.; Ruzsinszky, A.; Csonka, G. I.; Vydrov, O. A.; Scuseria, G. E.; Constantin, L. A.; Zhou, X.; Burke, K. *Phys. Rev. Lett.* **2008**, *100*, 136406.

(39) van Lenthe, E.; Baerends, E. J.; Snijders, J. G. *J. Chem. Phys.* **1994**, *101*, 9783–9792.

(40) Head, J. D.; Zerner, M. C. *Chem. Phys. Lett.* **1985**, *122*, 264 – 270.

(41) Payne, D. J.; Egdell, R. G.; Walsh, A.; Watson, G. W.; Guo, J.; Glans, P.-A.; Learmonth, T.; Smith, K. E. *Phys. Rev. Lett.* **2006**, *96*, 157403.

(42) Mariano, A. N.; Chopra, K. L. *Appl. Phys. Lett.* **1967**, *10*, 282–284.

(43) Chattopadhyay, T.; Pannetier, J.; Von Schnering, H. G. *J. Phys. Chem. Solids* **1986**, *47*, 879–885.

(44) Badachhape, S.; Goswami, A. *J.Phys. Soc. Jpn, Suppl. B2 ,* **1962**, *17*, 251–253.

(45) Bilenkii, B.; Mikolaichuk, A.; Freik, D. *Physica Status Solidi* **1968**, *28*, K5–K7.

(46) Arora, S. K.; Patel, D. H.; Agarwal, M. K. *Cryst. Res. Technol.* **1993**, *28*, 623–627.

(47) Moore, W. J.; Pauling, L. *J. Am. Chem. Soc.* **1941**, *63*, 1392–1394.

(48) Baur, W. H.; Khan, A. A. *Acta Crystallogr. Sect. B: Struct. Sci.* **1971**, *27*, 2133–2139.

(49) Wiedemeier, H.; Csillag, F. J. *Z. Kristallogr.* **1979**, *149*, 17.

(50) Kresse, G.; FurthmÃijller, J. *Phys. Rev. B* **1996**, *54*, 11169 – 11186.

(51) Scragg, J. J.; Dale, P. J.; Colombara, D.; Peter, L. M. *ChemPhysChem* **2012**, *13*, 3035–3046.

(52) *CRC Handbook of Chemistry and Physics*, 92nd ed.; CRC Press: Boca Raton, FL, 2011-2012.

(53) Sharma, R.; Chang, Y. *J. Phase Equilib.* **1986**, *7*, 269–273.

(54) Novoselova, A. V.; Zlomanov, V. P.; Karbanov, S. G.; Matveyev, O. V.; Gas'kov, A. M. *Prog. Solid State Chem.* **1972**, *7*, 85 – 115.

(55) Piacente, V.; Foglia, S.; Scardala, P. *ChemInform* **1992**, *23*, no.

(56) TanuÃĚÂąevski, A.; Poelman, D. *Sol. Energ. Mat. Sol. C.* **2003**, *80*, 297 – 303.

(57) Burton, L. A.; Walsh, A. *J. Solid State Chem.* **2012**, in press.

(58) Stoltzfus, M. W.; Woodward, P. M.; Seshadri, R.; Klepeis, J.-H.; Bursten, B. *Inorg. Chem.* **2007**, *46*, 3839–3850.

(59) Walsh, A.; Watson, G. W. *J. Phys. Chem. B* **2005**, *109*, 18868–18875.

(60) Lefebvre, I.; Szymanski, M. A.; Olivier-Fourcade, J.; Jumas, J. C. *Phys. Rev. B* **1998**, *58*, 1896–1906.

(61) Scanlon, D. O.; Walsh, A. *Applied Physics Letters* **2012**, *100*, 251911.

(62) Momma, K.; Izumi, F. *J. Appl. Crystallogr.* **2011**, *44*, 1272–1276.